nature communications

Article | Article in Press

https://doi.org/10.1038/s41467-026-79566-7

Expansion of North Atlantic Deep Water during Northern Hemisphere Glaciation

Received: 8 December 2025

Accepted: 22 October 2026

Published online: 17 November 2026

Check for updates

Friso de Graaf[1,2,3] ✉, David Thornalley[2], David J. Wilson[3], Zarina Hewett[2,3,4], Yair Rosenthal[5], Stella Woodard[5,6] & Heather L. Ford[1]

Atlantic Meridional Overturning Circulation (AMOC) is a major driver of the Earth's climate, moving heat from the Southern Hemisphere to the Northern Hemisphere. Neither foraminiferal carbon isotope records nor modelling studies agree on the spatial extent of North Atlantic Deep Water (NADW), the northern deep limb of the AMOC, over the intensification of Northern Hemisphere Glaciation (iNHG, ~2.73 million years ago). Here we present high-resolution neodymium isotope (ε_{Nd}) records from a depth transect in the equatorial Atlantic over the iNHG. We find a persistent latitudinal and depth gradient in neodymium isotope values in the deep Atlantic during the Late Pliocene, absent in the Early Pleistocene, indicating an expansion of NADW extent over the iNHG. In contrast, our reconstruction suggests very little glacial-interglacial variability in NADW extent during both the Late Pliocene and Early Pleistocene. These results suggest deep-water circulation was substantially different during a warm climate state, with implications for the role of NADW formation during major climate transitions and its future stability.

Understanding ocean circulation is vital for making accurate projections of future climate. The Atlantic Meridional Overturning Circulation (AMOC) is an important ocean circulation pathway, forming deep waters in the high-latitude North Atlantic, which are then exported southwards, ultimately returning as surface waters[1]. The AMOC is responsible for substantial movement of heat from the Southern Hemisphere to the Northern Hemisphere[2], and modelling studies have shown that reductions in AMOC strength can lead to major climatic changes[3]. Despite its importance, poor constraints on the nature of the AMOC in a future warmer world represent a source of uncertainty in climate projections[4,5].

The northern branch of the AMOC is represented by North Atlantic Deep Water (NADW), which forms in the high latitudes of the North Atlantic and is transported southwards. Antarctic Bottom Water (AABW) represents the southern branch that forms in the Southern Ocean and is transported northwards, where it occupies the deepest Atlantic[1]. Both AABW and NADW interact to shape the overall structure of the AMOC. All else being equal, a stronger AMOC would result in a greater NADW extent and, therefore, NADW extent could be used as a proxy for AMOC strength in the past. However, greater NADW extent could also be driven by changes in the relative densities of NADW and southern-sourced water masses or by decreased strength of AABW export[6].

Changes in past ocean circulation can be tracked using tracers, including carbon and neodymium isotopes. Carbon isotope ratios ($\delta^{13}C$) in the tests of benthic foraminifera have traditionally been used as a proxy for relative water mass proportions due to the semi-conservative nature of $\delta^{13}C$ values in seawater[7]. High $\delta^{13}C$ values are associated with the northern-sourced endmember in the deep Atlantic, NADW, whereas the modern southern-sourced endmember, AABW, has lower $\delta^{13}C$ values[8]. Shifts in deep Atlantic benthic $\delta^{13}C$ records towards lower values during past glacial intervals were traditionally interpreted to indicate an increased presence of AABW and a reduction in NADW extent[6,9]. However, changes in surface-ocean

[1]School of Geography, Queen Mary University of London, London, UK. [2]Department of Geography, University College London, London, UK. [3]Department of Earth Sciences, University College London, London, UK. [4]School of Earth and Environmental Sciences, Cardiff University, Cardiff, UK. [5]Department of Marine and Coastal Sciences, Rutgers, The State University of New Jersey, New Brunswick, NJ, USA. [6]Global Aquatic Research LLC, Sodus, NY, USA.
✉e-mail: f.m.degraaf@qmul.ac.uk

productivity and the rate of remineralisation of organic carbon along water mass pathways can alter the $\delta^{13}C$ signatures of water masses[7,10], while changes in ventilation processes in the source regions of deep water masses can change endmember $\delta^{13}C$ values[11], leading to uncertainty and potential bias in such interpretations.

In contrast, neodymium isotope ratios, as recorded in fish teeth or other authigenic deposits, can be used as an abiotic water mass tracer that is unaffected by changes in biological productivity or air-sea gas exchange[12,13]. Neodymium isotope ratios are expressed as ε_{Nd} values, giving the difference in the $^{143}Nd/^{144}Nd$ ratio between a sample and the chondritic uniform reservoir in parts per 10,000[12]. In general, unradiogenic (more negative) values are sourced from the North Atlantic and radiogenic (more positive) values are sourced from the Southern Ocean[13]. In the modern deep Atlantic, there is a divide in ε_{Nd} values corresponding to the boundary between NADW and AABW. The NADW is characterised by ε_{Nd} values below −12.4, with upper and lower NADW water masses having characteristic ε_{Nd} values of −13.2 and −12.4, respectively[14], while AABW is characterised by more radiogenic ε_{Nd} values above −9.6[15].

Notably, recent neodymium isotope studies have shown that both carbon isotopes and neodymium isotopes were considerably influenced by changes in water mass endmember values during Late Pleistocene glacial intervals, leading to the conclusion that NADW extent in the Atlantic Ocean did not markedly change between glacial and interglacial intervals[16,17].

The transition from the warm Late Pliocene to the Early Pleistocene was marked by global cooling and, due to the growth of ice sheets across the Northern Hemisphere, is known as the intensification of Northern Hemisphere Glaciation (iNHG, 2.73 Ma)[18] The iNHG is a major secular shift in the Earth's climate and offers an opportunity to understand AMOC structure during a climate in transition. During the warm Late Pliocene, several carbon isotope records suggest that NADW was more spatially extensive relative to the modern structure[19–21], which could be indicative of intensified overturning[19,20]. However, modelling studies are less clear, with the PlioMIP2 ensemble suggesting intensified AMOC overturning during the Late Pliocene relative to the modern, but with little agreement on the lateral or vertical NADW extent[22,23]. In CMIP6 models, stronger AMOC overturning strength is related to greater NADW (vertical) extent[24]; however, given uncertainties in the overturning strength of other regions of the global oceans over this period, and particularly the Southern Ocean, a stronger AMOC may not directly relate to an enhanced NADW extent. Such data-model discrepancies are a considerable gap in our understanding of AMOC intensity and structure during the recent global warming period. Over the iNHG, a shift to lower $\delta^{13}C$ values in the deep Atlantic suggests a reduction in NADW extent, though the mechanism for this change is uncertain[25–27], while other carbon isotope studies suggest that NADW extent may have been greater during interglacial intervals after the iNHG, but was reduced during glacial intervals of the Early Pleistocene[28,29]. Despite the major climatic changes over the iNHG[18], the current paradigm from Earth system models is that ocean circulation remained largely unchanged over this interval[22].

This study presents a suite of neodymium isotope records from a depth transect in the Equatorial Atlantic that can resolve glacial–interglacial variability before and after the iNHG. Ocean Drilling Program (ODP) Sites 925, 927 and 929 on the Ceará Rise (Fig. 1) are near the present-day boundary between AABW and NADW[14,30] (Fig. 2). We compare our records to an existing neodymium isotope record from IODP Site U1313 at 3426 m depth in the Northeast Atlantic Ocean[31,32] (Fig. 1), which we use to represent the composition of NADW near its formation regions. The composition of AABW over this interval is represented by records from ODP Site 1123 in the South Pacific and ODP Site 704 and an existing record from ODP Site 1267 in the Southeast Atlantic Ocean[32] (Fig. 1). Our results reveal a pronounced ε_{Nd} gradient between the North and Equatorial Atlantic in the Late Pliocene that is absent during both glacial and interglacial intervals of the Early Pleistocene (Fig. 3), indicating a more restricted NADW spatial extent during the Late Pliocene that expanded over the iNHG.

Results and discussion

Reduced the North Atlantic Deep Water extent during the Late Pliocene

In the Late Pliocene, NADW shoaled in the Equatorial Atlantic relative to the present. There is a significant difference ($P = 0.005$) in the ε_{Nd} values between ODP 925 (3042 m depth) and the deeper sites ODP 927 (3313 m depth) and 929 (4357 m depth) across all intervals in the Late Pliocene (Fig. 3), but no difference between the two deeper sites ($P = 0.33$). This persistent vertical gradient in ε_{Nd} values through both glacial and interglacial intervals in the Late Pliocene (Fig. 4) indicates vertical water mass stratification of the Atlantic Ocean over this period. This feature suggests that NADW was shallower in the Late Pliocene, with the lower boundary at ~3000 m depth in the Equatorial Atlantic Ocean, compared to ~4000 m depth in both the present (Fig. 2) and the Late Pleistocene[33]. There is a convergence in ε_{Nd} values between Ceará Rise sites during MIS KM3 (3.16 Ma), which, despite limited data coverage, appears to have been driven by a shift in ε_{Nd} values at ODP 925 towards more radiogenic values (Fig. 3). This feature could imply an even greater shoaling of NADW extent during MIS KM3 to above 3000 m depth.

In addition to the shallower NADW extent, our results also show a latitudinal gradient in ε_{Nd} values in the deep North Atlantic between 41°N (IODP U1313) and 4°N (Ceará Rise) (Figs. 3 and 4), indicating that NADW did not extend as far south as the equator (at least not without considerable mixing with another water mass) during the Late Pliocene. There is a significant difference ($P < 10^{-10}$) between the ε_{Nd} values from the three sites on the Ceará Rise and IODP U1313 in the North Atlantic[31] (Fig. 3), with an approximately 1 ε-unit offset. This difference persisted for both glacial and interglacial intervals of the Late Pliocene (Fig. 4). The gradient between IODP U1313 and the Ceará Rise sites is not seen in the Early Pleistocene, with no significant difference between IODP U1313 and the Ceará Rise sites in the Early Pleistocene ($P = 0.6673$, Fig. 3). The stronger gradient between the North and Equatorial Atlantic Ocean in the Pleistocene could be explained by a change in ε_{Nd} endmembers, or by the emergence of a water mass boundary between these regions, with a different mixture of water masses occupying the deep North and Equatorial Atlantic Ocean in the Late Pliocene.

The stronger latitudinal gradient in ε_{Nd} values in the deep North Atlantic could also be the result of slower overturning in the Late Pliocene. Slower overturning would lead to longer residence times in the deep Atlantic and a greater impact of benthic flux on the deep Equatorial Atlantic ε_{Nd} values[34,35]. A stronger benthic flux control at the Ceará Rise relative to IODP U1313 could result in a more radiogenic signal at the Ceará Rise, as observed in the Late Pliocene (Fig. 3), provided that benthic sediments along the deep North Atlantic flow path were more radiogenic than the water. In the modern day, detrital ε_{Nd} values from the deep Atlantic are more unradiogenic than the overlying water mass[36]. In order for the stronger latitudinal gradient in ε_{Nd} values in the deep North Atlantic to be caused by a weaker AMOC overturning strength, without a reduction in NADW extent, the detrital ε_{Nd} signal would need to have been considerably more radiogenic in the Late Pliocene than in the modern day. Hence, this idea is not supported by the existing data but could be tested by future studies on detrital records. We therefore favour the former interpretation of a reduced Pliocene NADW extent, while noting that the alternative interpretation of weaker AMOC overturning would still represent a departure from the interpretations of most carbon isotope records[19,20] and modelling studies[22] for the Late Pliocene deep Atlantic Ocean. It is

https://doi.org/10.1038/s41467-026-79566-7

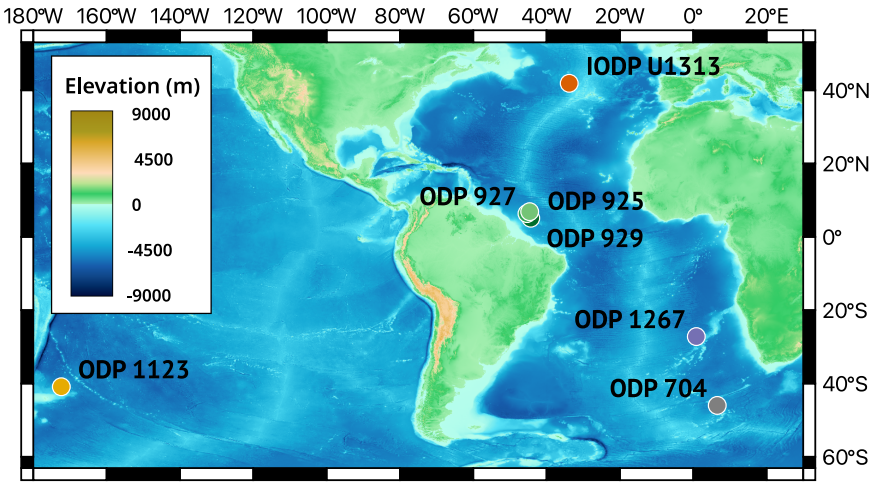


Fig. 1 | Map showing the locations of the core sites. Bathymetric map of the Atlantic and Pacific Oceans showing the location of ODP Sites 925, 927 and 929 on the Ceará Rise, ODP 1123 in the South Pacific, ODP 704 and 1267 in the Southeast Atlantic and IODP U1313 in the Northeast Atlantic. The map was made from data available in ref. 83.

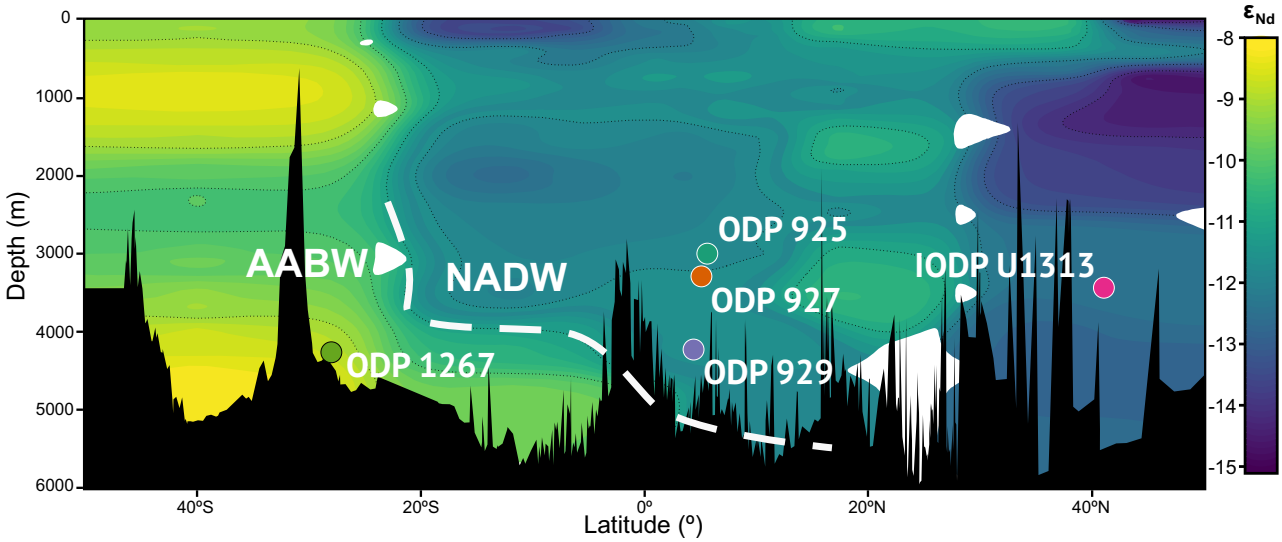


Fig. 2 | Neodymium isotope composition of the modern Atlantic Ocean. Atlantic seawater ε_{Nd} values from the GEOTRACES project[63] along a section from 50°N, 50°W to 50°S, 30°W, including all data points for 1000 km either side. The locations of the three core sites on the Ceará Rise, IODP U1313 and ODP 1267 are shown. Note that ODP 1267 is located in the Angola Basin in the Southeast Atlantic which is fed by waters which flow over the Romanche and Rio de Janeiro Fracture Zones and thus is bathed in waters from further north at around 20°S[32]. The approximate boundary between NADW and AABW, defined as $\varepsilon_{Nd} = -11.2$ in agreement with ref. 14, is drawn with a white dashed line. The section was made in Ocean Data View[84].

also feasible that a reduced NADW extent and weaker AMOC overturning acted synergistically to generate the observed ε_{Nd} gradients.

The depth gradient in ε_{Nd} values in the Late Pliocene Atlantic was unlikely to have been driven by a reduction in Atlantic overturning speed. In principle, slower overturning in the Pliocene deep Atlantic could have created a stronger depth contrast in ε_{Nd} values, as signals supplied from benthic flux at abyssal depths would have a greater capacity to mix with the water masses of the deep Atlantic Ocean[37]. However, while there is a strong ε_{Nd} gradient between ODP 925 (3042 m depth) and ODP 927 (3313 m depth) in the Pliocene, there is no significant difference between ODP 927 and ODP 929 (4357 m depth) (Fig. 3), as would be expected if these changes were driven by slower deep ocean overturning in the Late Pliocene.

The depth and latitudinal gradients in ε_{Nd} values observed during the Late Pliocene are also unlikely to have been the result of shifts in the ε_{Nd} composition of NADW due to changes in the relative strength of its constituents (e.g. a reduction in Labrador Sea input into NADW). Labrador Sea Water (LSW) is a component of NADW that is characterised by very negative ε_{Nd} values around −13.5[14,38]. In the modern day, LSW extends to 1500 m depth[14], but a deeper and more spatially extensive LSW could potentially generate the spatial gradient in ε_{Nd} values between IODP U1313, which would be bathed in a greater proportion of LSW relative to the deeper, more southern sites on the Ceará Rise. However, it is unlikely that an expansion of LSW would have caused the difference in ε_{Nd} values between Site U1313 and the Ceará Rise (the latitudinal gradient) without the emergence of a water mass boundary separating these sites from each other. Furthermore, LSW formation is expected to be weaker during warmer climates[39,40], such as in the Late Pliocene. A reduction in the LSW formation and a reduced LSW contribution to NADW would give NADW a more positive ε_{Nd} value without any change in the location of the NADW-AABW water mass boundary, which may have contributed to the more positive ε_{Nd} values observed across the deep North Atlantic in the Late Pliocene compared to the Late Pleistocene (Fig. 5).

https://doi.org/10.1038/s41467-026-79566-7

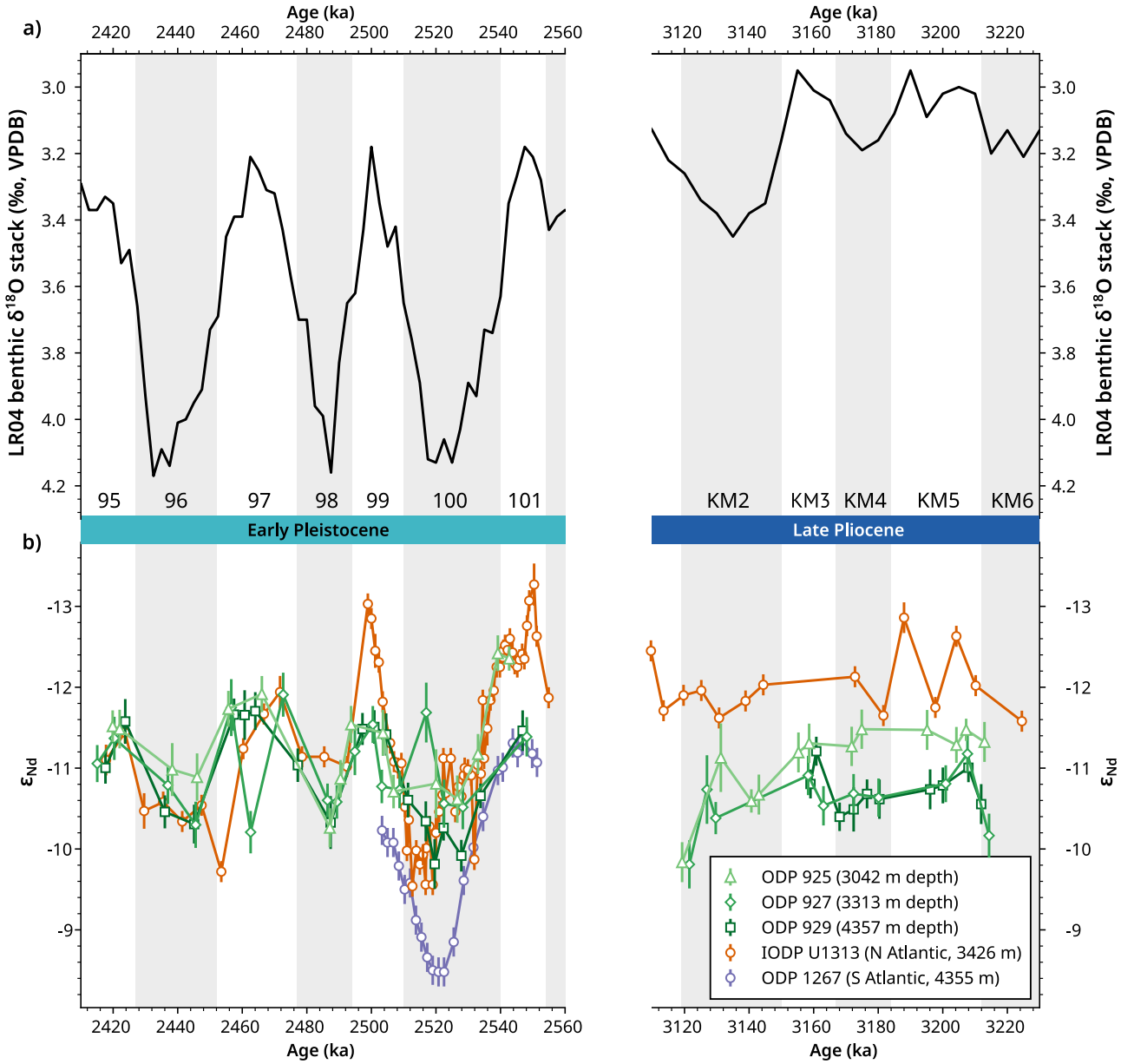


Fig. 3 | Neodymium isotope records from the Late Pliocene and Early Pleistocene. a LR04 benthic $\delta^{18}O$ stack[79] from the Late Pliocene (right) and Early Pleistocene (left). **b** Neodymium isotope data (ε_{Nd}) from Sites ODP 925 (triangles), 927 (diamonds), and 929 (squares) on the Ceará Rise, and from IODP Site U1313[31,32] (orange circles) in the Northeast Atlantic and ODP Site 1267[32] (purple circles) in the Southeast Atlantic Ocean. All data are shown with ±2σ error bars. Glacial intervals in grey bars are based on the LR04 stacked $\delta^{18}O$ record[79] and Marine Isotope Stages are annotated.

The difference in ε_{Nd} values between the shallower and deeper Ceará Rise sites in the Pliocene deep Atlantic is most easily explained by a reduction in NADW extent. A more unradiogenic NADW or a more radiogenic AABW could amplify any existing ε_{Nd} gradients, but would not explain the appearance of a gradient in ε_{Nd} values between ODP 925 and ODP 927 and 929. In addition, there is no evidence of a more unradiogenic NADW water mass in the Late Pliocene[31,32], and our results from ODP 1123 and 704 indicate a similarly radiogenic water mass in the Southern Pacific in the Late Pliocene relative to the Late Pleistocene[41] (Fig. 5). The ε_{Nd} values from both ODP 1123 and 704 and from ferromanganese crusts in the Southern Ocean[42] show no significant trend from 3.3 to 2.9 Ma, which suggests that this southern-sourced water mass does not change in ε_{Nd} composition over this interval (Supplementary Fig. 1). However, neither the ferromanganese crusts nor fish teeth data are of sufficiently high resolution to determine glacial–interglacial variations in the AABW endmember over this period, with only two data points from 3.22 to 3.10 Ma, which limits our ability to quantitatively estimate water mass proportions in the Equatorial Atlantic. The offset between ε_{Nd} values from the Equatorial and North Atlantic throughout the Late Pliocene also suggests that these data are unlikely to be the result of diagenetic alteration or regional processes such as benthic flux or reversible scavenging[37,43]. However, this difference is not present for the entirety of the Late Pliocene (Fig. 3), and therefore it is impossible to state conclusively that benthic flux is not responsible for the depth gradient in ε_{Nd} values.

The Pliocene reduction in NADW extent could be the result of a reduction in NADW formation and/or production of less dense NADW. North Atlantic sea surface temperature records from the Late Pliocene show much warmer temperatures than the rest of the world's oceans[44]

https://doi.org/10.1038/s41467-026-79566-7

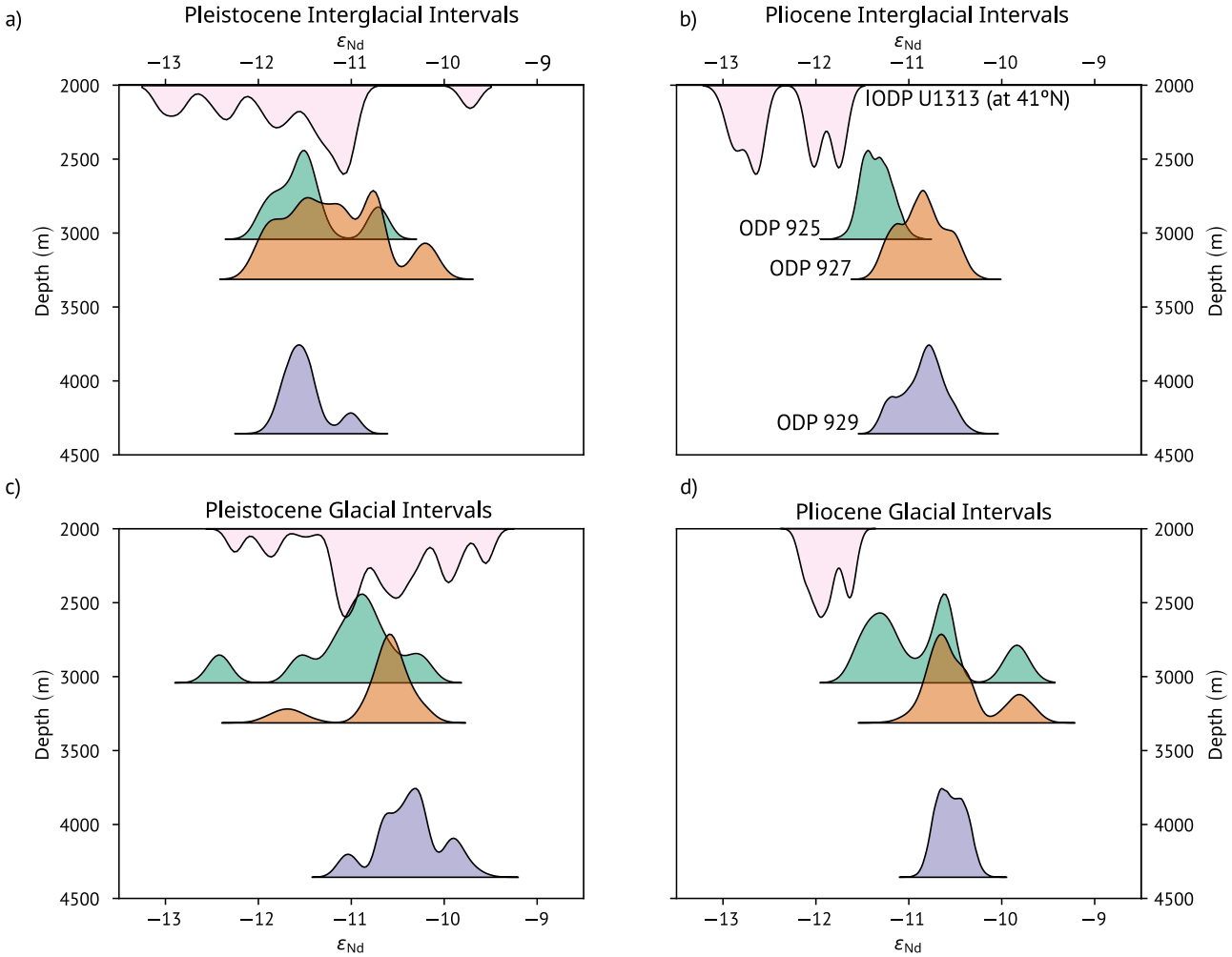


Fig. 4 | Neodymium isotopes in a depth transect across the Ceará Rise. Probability density functions showing the distribution of ε_{Nd} values against depth for ODP Sites 925 (green), 927 (orange) and 929 (purple) on the Ceará Rise during **a** Pleistocene interglacials, **b** Pliocene interglacials, **c** Pleistocene glacials and **d** Pliocene glacials. Note that the Pleistocene interglacial data excludes data from MIS 101. The distribution of ε_{Nd} values from North Atlantic IODP Site U1313 (3426 m depth)[31,32] for the same time intervals as the Ceará Rise distributions is shown in pink at the top of each panel (U1313 is located in the North Atlantic at 41°N, compared to the Ceará Rise sites at 5°N, and is therefore not plotted at 3426 m depth).

and this warmth would inhibit deep water formation. This hypothesis is supported by records of North Atlantic bottom-water temperature (BWT), which suggest that NADW was a much warmer[45], and thus less dense, water mass in the Pliocene. Alternatively, there is strong evidence for a Late Pliocene meridional overturning circulation in the Pacific Ocean[46–48], and modelling studies suggest that active overturning in the Pacific could weaken overturning circulation in the Atlantic Ocean by reducing the transport of dense saline surface waters to the North Atlantic and, instead, rerouting these to the North Pacific[49–51].

Processes driving variability of AMOC after the iNHG

After the iNHG, there is a convergence of neodymium isotope values across the Northern and Equatorial Atlantic (Fig. 4). From MIS 100 (2.54 Ma) onwards, there is no significant difference ($P = 0.67$) between the ε_{Nd} values from the Ceará Rise and those from IODP U1313 (Fig. 3), nor any difference between the ε_{Nd} records from any of the Ceará Rise sites themselves ($P = 0.24$) over the Early Pleistocene. The convergence of ε_{Nd} values suggests that a similar water mass was bathing all sites, which was most likely an expanded NADW that extended to at least 4300 m depth in the Equatorial Atlantic (Fig. 6). Notably, there is a >1 ε-unit difference between the Ceará Rise ε_{Nd} values and those from South Atlantic Site ODP 1267[30] during MIS 100 (Fig. 3), which suggests that the convergence in ε_{Nd} values is not due to an expansion of southern-sourced AABW, as previously suggested[31].

The expansion of the NADW extent after the iNHG was most likely driven by an increase in AMOC strength. An expansion of ice sheets and sea-ice extent in the Northern Hemisphere would cool the North Atlantic, while sea-ice formation in the North Atlantic could precondition the ocean for deep water formation by increasing the surface-layer salinity via brine rejection, as occurs in the Greenland Sea today[52]. Both of those processes would serve to increase NADW formation in the Early Pleistocene, and such a change would help to explain the decrease in BWT in the deep Atlantic after the iNHG[45]. A convergence in BWT between the Atlantic and Pacific after the iNHG has been linked to better water mass mixing between basins[53], and a more extensive NADW after the iNHG would support this hypothesis. The ε_{Nd} values at ODP 1123 do not show a clear shift towards more unradiogenic values after the iNHG (Fig. 5) as would be expected for an increased NADW export into the Southern Ocean, although the record from ODP 1123 does not extend much younger than MIS 100 (Fig. 5).

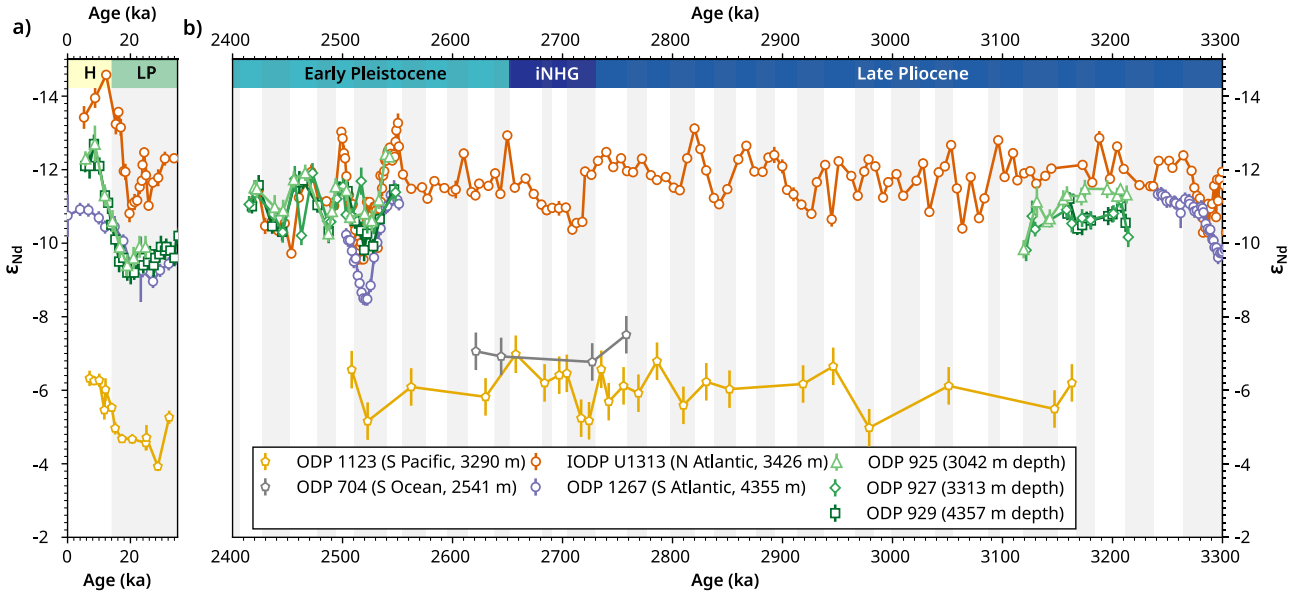


Fig. 5 | Comparison of the neodymium isotope records across the iNHG and the Late Pleistocene. a Neodymium isotope data (ε_{Nd}) from Sites ODP 925[61], 929[62], 1123[41], 1267[32] and IODP Site U1313[31] for the Late Pleistocene and Holocene. **b** Neodymium isotope data (ε_{Nd}) from Sites ODP 925, 927, 929, and 1123, and from ODP Site 1267[32] and IODP Site U1313[31,32] for the Late Pliocene and Early Pleistocene. All data are shown with ±2σ error bars. H Holocene, LP Late Pleistocene.

Maximal NADW extent during the Early Pleistocene

All the sites in the Equatorial and North Atlantic exhibit glacial–interglacial variability in ε_{Nd} values in the Early Pleistocene, driven by changes in endmember ε_{Nd} values. In the Early Pleistocene, there is a 1 ε-unit shift in ε_{Nd} values from glacial to interglacial intervals that is seen across the North and Equatorial Atlantic (Fig. 3), but there is no significant difference in the ε_{Nd} values between sites on the Ceará Rise ($P = 0.235$) or between IODP U1313 and the Ceará Rise sites ($P = 0.667$) over the Early Pleistocene. This finding could potentially imply that all sites were bathed in the same southern-sourced water mass during glacial intervals and the same northern-sourced water mass during interglacial intervals, but a similar glacial–interglacial shift in ε_{Nd} values is also seen at ODP 1267[32] at more radiogenic values, which indicates a persistently larger southern sourced contribution to the South Atlantic (Fig. 3). This spatial pattern suggests that there was no major change in the deep water mass structure from glacial to interglacial intervals (Fig. 6), but a change in the endmember ε_{Nd} values of NADW or AABW. Without high-resolution records from the Southern Ocean in the Early Pleistocene, it is difficult to say which endmember is dominantly driving this change. The more radiogenic ε_{Nd} values during Early Pleistocene glacial intervals in the North and Equatorial Atlantic could be the result of reduced weathering of old cratonic material on the North American continent due to the presence of large ice sheets, which would reduce the supply of highly unradiogenic sediment to the Labrador Sea, shifting NADW towards more radiogenic ε_{Nd} values akin to Late Pleistocene glacial intervals[54–56].

In the Late Pleistocene, there is a 1 ε-unit gradient between IODP U1313 and the sites on the Ceará Rise, but there is no gradient in ε_{Nd} values between ODP 925 and 929 (Fig. 5). We suggest that there was a reduction in NADW extent in the Late Pleistocene relative to the Early Pleistocene, with IODP U1313 and the Ceará Rise sites bathed in a different mixture of water masses in the Late Pleistocene. The maximum NADW extent in the Early Pleistocene may have been driven by cooling temperatures relative to the Pliocene, but without the freshwater forcing from more expansive Late Pleistocene ice growth. The reduction in NADW extent for the cooler Late Pleistocene may also relate to a rebalancing of the relative strengths of NADW and AABW linked to changes in inter-basin heat transport[57], and/or stronger, denser AABW formation linked to increased sea-ice formation in a colder climate[58].

In summary, our results point to a different deep-water structure in the Atlantic Ocean during the warm Late Pliocene, one which is not seen in the Pleistocene. We suggest that the NADW extent was markedly reduced in the Pliocene, and that it expanded only after the iNHG. The AMOC is a crucial part of the global ocean circulation and plays a vital role in moderating the climate of the Northern Hemisphere[59]. Given that CMIP6 models suggest NADW (vertical) extent is related to AMOC strength[24], our results may support the idea of a weaker AMOC during the warm climate of the late Pliocene. Future work should investigate the underlying mechanism(s), including changes in boundary conditions like oceanic gateways, and whether it is attributable to the existence of a Pliocene PMOC, or whether it is an integral response to the warmer climate.

Methods

Site location

A total of 86 samples were taken from ODP Sites 925, 927 and 929 on the Ceará Rise in the Equatorial Atlantic (Fig. 1 and Supplementary Table 1), which were collected on ODP Leg 154[60]. The Holocene core-top authigenic ε_{Nd} values of planktic foraminifera from ODP Sites 925[61] and 929[62] agree with modern seawater measurements[63], which suggests that authigenic ε_{Nd} measurements from cores on the Ceará Rise reliably record bottom water compositions. A further 24 samples were taken from ODP Site 1123 in the Southern Pacific Ocean (Fig. 1), which was collected on ODP Leg 181[64], and 4 samples were taken from ODP Site 704 in the Southern Ocean (Fig. 1), which was collected on ODP Leg 114[65].

Sediment cores with a high carbonate content are unlikely to be affected by detrital contamination of porewater neodymium isotope signals[66]. All three sites on the Ceará Rise have relatively high carbonate content, with around 30% $CaCO_3$ in the Holocene, and, crucially, higher proportions of around 50–60% $CaCO_3$ in the Late Pliocene and Early Pleistocene[30,67]. The Ceará Rise is an aseismic ridge off the coast of Brazil that is around 800 km from the mouth of the Amazon River. Therefore, records from this location could potentially have been

https://doi.org/10.1038/s41467-026-79566-7

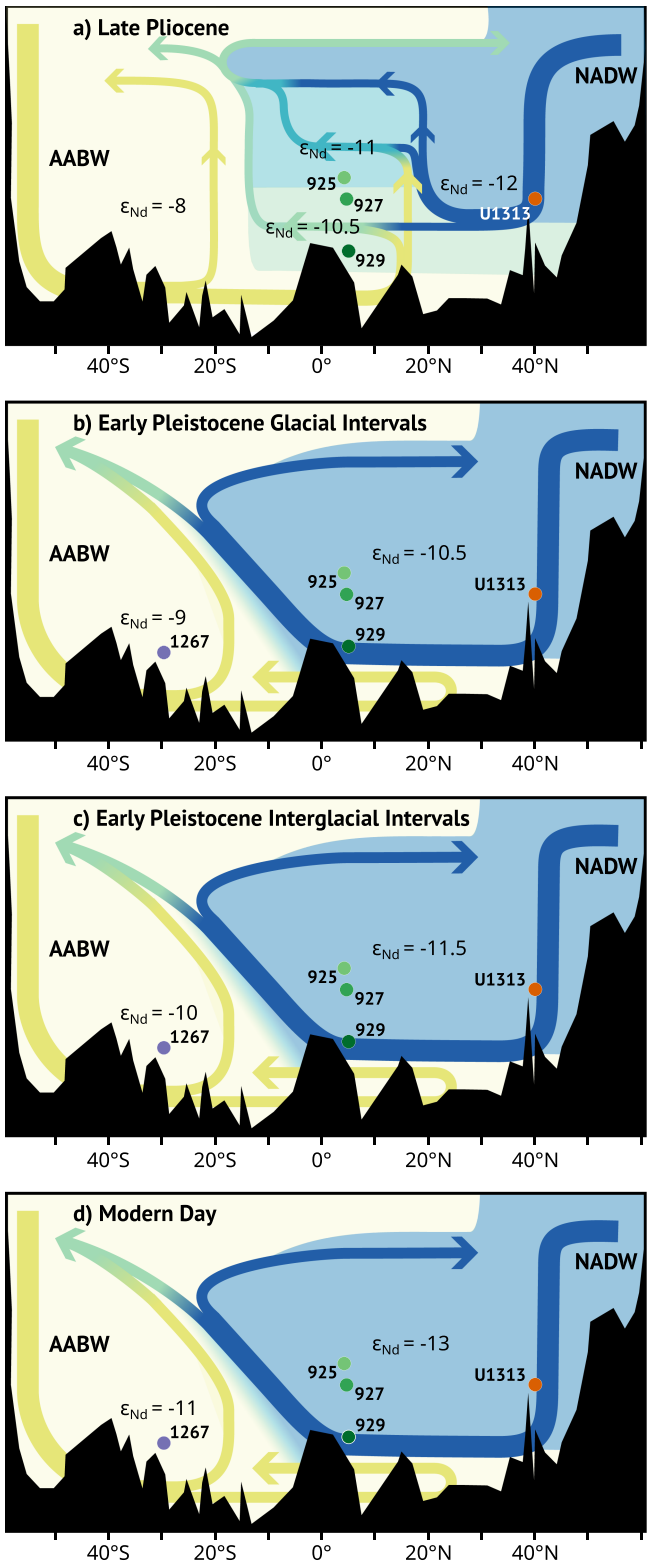


Fig. 6 | Schematic showing deep Atlantic water mass structure in the Late Pliocene and Early Pleistocene. a Water mass structure during the Late Pliocene for the same section as in Fig. 2, showing a reduced North Atlantic Deep Water (NADW) extent and diffuse water mass boundaries. **b** Water mass structure for the Early Pleistocene glacial intervals, showing an expanded NADW extending down to 4000 m depth in the Equatorial Atlantic, replacing Antarctic Bottom Water (AABW). **c** Water mass structure for Early Pleistocene interglacial intervals, which is very similar to glacial intervals. **d** Water mass structure for the modern day with a structure similar to the Early Pleistocene glacial and interglacial intervals. Estimates of ε_{Nd} values for water masses are annotated, with Late Pliocene South Atlantic estimates from ferromanganese crust data at Site MW8801 D18-1 in the Southern Ocean[42].

influenced by terrigenous runoff from the Amazon. While there is considerable terrigenous sediment in the region that is sourced from the Amazon, the sediment on the Ceará Rise is primarily pelagic in origin[68]. There are suggestions that there may have been high sediment transport from the Amazon to the Ceará Rise during the Late Oligocene and Early Miocene, but the evidence for this transport shows it fading by 8.7 Ma[69]. In the present, bulk sediment ε_{Nd} measurements from the Amazon Fan show no influence of Amazonian sediment reaching as far as the Ceará Rise[70]. For this reason, we discount the possibility of serious terrigenous influence on the Pliocene-Pleistocene ε_{Nd} signal from ODP 925, 927, and 929.

Similarly, for ODP 1123, located on the Chatham Rise in the South Pacific, the carbonate content varies between 50 and 80% for most of the Late Pliocene and Early Pleistocene[71]. The site is situated on a sediment drift formed by the slowing of the deep western boundary current as it passes New Zealand, which carries terrigenous sediment to the site from the Solander and Bounty Channels[72]. Such inputs could potentially result in an alteration of the authigenic ε_{Nd} signal towards more terrestrial ε_{Nd} values. The Solander and Bounty Channels are predominantly fed by erosion and weathering of radiogenic ocean island basalts and granitoids on New Zealand, with ε_{Nd} values ranging from −5 to +8[73,74]. Therefore, while there may have been a terrigenous influence on the ε_{Nd} values recorded at ODP 1123, it would be expected to have made the values more radiogenic, not less radiogenic as observed.

ODP Site 704 is located in the eastern subantarctic South Atlantic Ocean and has a carbonate content that ranges from 60 to 85% throughout the Late Pliocene[75]. The site is located far from any sources of terrigenous sediment, and while there are influxes of IRD, these peaks occur at 4.4 and 3.6 Ma[75] and thus are unlikely to impact the neodymium isotope record.

Neodymium isotope measurements

Samples from ODP Sites 925 (30 samples), 927 (27 samples) and 929 (29 samples) were analysed for fish-teeth neodymium isotope composition. Approximately ten pieces of fish teeth and bone were picked from the washed and dried coarse fraction (>150 µm) for each sample. These samples were then cleaned in three washes of ultrapure water (18.2 MΩ) with ultrasonication, three washes of ethanol with ultrasonication, and another 3 washes of ultrapure water with ultrasonication. A weak acid was added to the samples (0.001 M HNO_3) to remove any contaminants. The samples were then dissolved in 3 M HCl and dried down.

For ODP Site 1123 (24 samples) and 704 (4 samples), ~20–30 fish teeth were picked from the >63 µm fraction. These samples were then cleaned in three washes of ultrapure water (18.2 MΩ) with ultrasonication, three washes of ethanol with ultrasonication, and another three washes of ultrapure water with ultrasonication. A weak acid was added to the samples (0.001 M HNO_3) to remove any contaminants, and then the samples were dissolved in 2 M HNO_3 and dried down.

The Nd in the samples was then isolated using a two-stage column chromatography process. For the Ceará Rise sites, an external BCR-2 rock standard, an internal multi-rare earth element standard, and a blank were also processed through the columns to determine reproducibility. For ODP Sites 1123 and 704, an internal rare earth standard and a blank were processed through the columns. The first column (10 mm diameter, 4 cm long, with 1.4 ml cation exchange resin AG50W X-8) was conditioned with 1 ml 1 M HCl. The samples were then loaded in 1 ml 1 M HCl, washed into the resin with 1 ml 1 M HCl, and eluted with 7 ml 3 M HCl and 0.5 ml 6 M HCl, before the REE were collected with 6.5 ml 6 M HCl and dried. The second column (4 mm diameter, 9.5 cm long, with 0.7 ml LN resin) was conditioned with 2 ml 0.2 M HCl, before the samples were loaded in 200 µl 0.2 M HCl and washed into the resin with 300 µl 0.2 M HCl. The samples were eluted with 5.5 ml 0.2 M HCl and then collected with 6 ml 0.2 M HCl. The samples were

dried down, and concentrated HNO_3 was added to remove any residue, after which the samples were refluxed and then dried down again.

The prepared Ceará Rise samples were diluted in 1 ml 2% HNO_3, and the neodymium isotope ratios ($^{143}Nd/^{144}Nd$) were measured in the LOGIC laboratory at University College London using a Nu Instruments Plasma 3 multi-collector inductively coupled plasma mass spectrometer (MC-ICP-MS) coupled to an Aridus 3 desolvating nebuliser system. Mass bias was corrected using the exponential law (to $^{146}Nd/^{144}Nd = 0.7219$). A correction for direct ^{144}Sm interference was also applied, with all samples significantly below the threshold determined for accurate correction (<0.1% of the ^{144}Nd signal). A total of 30 measurements were taken for each sample, with the mean and double standard error (2 s.e.) used as the measurement value and error. Each sample measurement was bracketed by JNdi-1 standards of matching concentration, and the data were adjusted to agree with the literature value[76]. External reproducibility was based on the standard deviation (2 s.d.) of the JNdi-1 standards run within the same part of the analytical session as the samples. The greater of the external or internal reproducibility was then used as the final error in the sample measurements. Column blanks contained on average 0.24 ± 0.24 ng of Nd ($n = 10$), compared to an average of 1960 ng of Nd in samples, and were thus considered negligible. The BCR-2 standards gave an average $^{143}Nd/^{144}Nd$ value of 0.512633 ± 0.000018 ($n = 10$), which is in good agreement with literature values of 0.512634 ± 0.000012[77] and gives a long-term reproducibility of 0.35 ε_{Nd} units.

The ODP 1123 and 704 samples were analysed using a similar method, with the neodymium isotope ratios measured on a Thermo Scientific Neptune Plus MC-ICP-MS in the Department of Earth and Planetary Sciences at Rutgers University. The JNdi-1 concentration-matched standards were only run after every seven sample runs rather than after every sample, with the data again adjusted to agree with the literature value[76]. External reproducibility was based on the standard deviation (2 s.d.) of all the JNdi-1 standards analysed alongside the samples. The greater of the external or internal reproducibility was then used as the final error in the sample measurements.

Age models

The age models for ODP Sites 925, 927 and 929 were from ref. 78 based on aligning the benthic oxygen isotopes to the LR04 stack. Marine isotope stages were picked manually based on the LR04 oxygen isotope curve[79]. The age model for ODP Site 1123 was from ref. 80 based on aligning benthic oxygen isotopes to the LR04 stack. The age model for ODP 704 was from ref. 79 and is part of the original LR04 oxygen isotope curve.

Statistical methods

The significance of any differences in the data was assessed using a standard independent two-sample Student *T* test. The data and errors in Fig. 4 were visualised using a Gaussian bootstrap sampling method[81] for the depth transects, with 10,000 sampling iterations per value without replacement. The code for this is available on GitHub in ref. 82.

Data availability

All data generated from sediment cores ODP 925, 927, 929, 1123 and 704 for this study have been made available in the Pangaea.de repository. Source data are provided with this paper.

Code availability

The code to generate the probability density functions in Fig. 4 is available on GitHub in ref. 82.

References

1. Talley, L. D. Closure of the global overturning circulation through the Indian, Pacific, and Southern Oceans: schematics and transports. *Oceanography* **26**, 80–97 (2013).
2. Johns, W. E. et al. Towards two decades of Atlantic Ocean mass and heat transports at 26.5. *N. Philos. Trans. R. Soc. Math. Phys. Eng. Sci.* **381**, 20220188 (2023).
3. Jackson, L. C. et al. Global and European climate impacts of a slowdown of the AMOC in a high resolution GCM. *Clim. Dyn.* **45**, 3299–3316 (2015).
4. Bellomo, K., Angeloni, M., Corti, S. & Von Hardenberg, J. Future climate change shaped by inter-model differences in Atlantic meridional overturning circulation response. *Nat. Commun.* **12**, 3659 (2021).
5. Jackson, L. C. et al. Challenges simulating the AMOC in climate models. *Philos. Trans. R. Soc. Math. Phys. Eng. Sci.* **381**, 20220187 (2023).
6. Adkins, J. F. The role of deep ocean circulation in setting glacial climates. *Paleoceanography* **28**, 539–561 (2013).
7. Ravelo, A. C. & Hillaire-Marcel, C. Chapter 18—The use of oxygen and carbon isotopes of foraminifera in paleoceanography. In *Developments in Marine Geology* (eds Hillaire–Marcel, C. & De Vernal, A.) 1 735–764 (Elsevier, 2007).
8. Lynch-Stieglitz, J. 6.16 Tracers of past ocean circulation. In *Treatise on Geochemistry* Vol. 6, 433–451 (Elsevier Pergamon, 2004).
9. Labeyrie, L. D. et al. Changes in the vertical structure of the North Atlantic Ocean between glacial and modern times. *Quat. Sci. Rev.* **11**, 401–413 (1992).
10. Gu, S. et al. Remineralization dominating the δ13C decrease in the mid-depth Atlantic during the last deglaciation. *Earth Planet. Sci. Lett.* **571**, 117106 (2021).
11. Oppo, D. W., Curry, W. B. & McManus, J. F. What do benthic δ13C and δ18O data tell us about Atlantic circulation during Heinrich Stadial 1? *Paleoceanography* **30**, 353–368 (2015).
12. Goldstein, S. L. & Hemming, S. R. Long-lived isotopic tracers in oceanography, paleoceanography, and ice-sheet dynamics. In *Treatise on Geochemistry* 453–489 https://doi.org/10.1016/B0-08-043751-6/06179-X (Elsevier, 2003).
13. van de Flierdt, T. et al. Neodymium in the oceans: a global database, a regional comparison and implications for palaeoceanographic research. *Philos. Trans. R. Soc. Math. Phys. Eng. Sci.* **374**, 20150293 (2016).
14. Lambelet, M. et al. Neodymium isotopic composition and concentration in the western North Atlantic Ocean: results from the GEOTRACES GA02 section. *Geochim. Cosmochim. Acta* **177**, 1–29 (2016).
15. Griffiths, A. et al. Neodymium isotope composition and rare earth element distribution of East Antarctic continental shelf and deep waters. *Chem. Geol.* **653**, 122039 (2024).
16. Pöppelmeier, F. et al. Northern-sourced water dominated the Atlantic Ocean during the Last Glacial Maximum. *Geology* **48**, 826–829 (2020).
17. Blaser, P. et al. Prevalent North Atlantic Deep Water during the Last Glacial Maximum and Heinrich Stadial 1. *Nat. Geosci.* https://doi.org/10.1038/s41561-025-01685-5 (2025).
18. McClymont, E. L. et al. Climate evolution through the onset and intensification of Northern Hemisphere Glaciation. *Rev. Geophys.* **61**, e2022RG000793 https://doi.org/10.1029/2022RG000793 (2023).
19. Raymo, M. E., Grant, B., Horowitz, M. & Rau, G. H. Mid-Pliocene warmth: stronger greenhouse and stronger conveyor. *Mar. Micropaleontol.* **27**, 313–326 (1996).
20. Ravelo, A. C. & Andreasen, D. H. Enhanced circulation during a warm period. *Geophys. Res. Lett.* **27**, 1001–1004 (2000).
21. Dowsett, H. J., Chandler, M. A. & Robinson, M. M. Surface temperatures of the Mid-Pliocene North Atlantic Ocean: implications for future climate. *Philos. Trans. R. Soc. Math. Phys. Eng. Sci.* **367**, 69–84 (2009).

22. Haywood, A. M. et al. The Pliocene Model Intercomparison Project Phase 2: large-scale climate features and climate sensitivity. *Clim. Past* **16**, 2095–2123 (2020).
23. Zhang, Z. et al. Mid-Pliocene Atlantic Meridional Overturning Circulation simulated in PlioMIP2. *Clim. Past* **17**, 529–543 (2021).
24. Nayak, M. S., Bonan, D. B., Newsom, E. R. & Thompson, A. F. Controls on the strength and structure of the Atlantic Meridional Overturning Circulation in climate models. *Geophys. Res. Lett.* **51**, e2024GL109055 (2024).
25. Hodell, D. A. & Venz, K. Toward a high-resolution stable isotopic record of the Southern Ocean during the Pliocene-Pleistocene (4.8 to 0.8 MA). In *Antarctic Research Series* (eds Kennett, J. P. & Warkne, D. A.) 265–310 https://doi.org/10.1029/AR056p0265 (American Geophysical Union, 1992).
26. Raymo, M. E., Hodell, D. & Jansen, E. Response of deep ocean circulation to initiation of northern hemisphere glaciation (3-2 MA). *Paleoceanography* **7**, 645–672 (1992).
27. Hodell, D. A. & Venz-Curtis, K. A. Late Neogene history of deep-water ventilation in the Southern Ocean. *Geochem. Geophys. Geosyst.* **7**, 2005GC001211 (2006).
28. Bell, D. B., Jung, S. J. A. & Kroon, D. The Plio-Pleistocene development of Atlantic deep-water circulation and its influence on climate trends. *Quat. Sci. Rev.* **123**, 265–282 (2015).
29. Karas, C. et al. Pliocene oceanic seaways and global climate. *Sci. Rep.* **7**, 39842 (2017).
30. Bickert, T., Cordes, R. & Wefer, G. 15. Late Pliocene to Mid-Pleistocene (2.6 - 1.0 Myr.) Carbonate dissolution in the Western Equatorial Atlantic: results of leg 154, Ceará Rise. In *Proceedings of the Ocean Drilling Program* (eds Shackleton, N. J., Curry, W. B., Richter, C. & Bralower, T. J.) 154, 229–237 (Integrated Ocean Drilling Program, 1997).
31. Lang, D. C. et al. Incursions of southern-sourced water into the deep North Atlantic during late Pliocene glacial intensification. *Nat. Geosci.* **9**, 375–379 (2016).
32. Kirby, N. et al. On climate and abyssal circulation in the Atlantic Ocean during late Pliocene marine isotope stage M2, c.3.3 million years ago. *Quat. Sci. Rev.* **250**, 106644 (2020).
33. Pöppelmeier, F., Jeltsch-Thömmes, A., Lippold, J., Joos, F. & Stocker, T. F. Multi-proxy constraints on Atlantic circulation dynamics since the last ice age. *Nat. Geosci.* **16**, 349–356 (2023).
34. Abbott, A. N., Haley, B. A. & McManus, J. Bottoms up: sedimentary control of the deep North Pacific Ocean's εNd signature. *Geology* **43**, 1035 (2015).
35. Haley, B. A., Du, J., Abbott, A. N. & McManus, J. The impact of benthic processes on rare earth element and neodymium isotope distributions in the oceans. *Front. Mar. Sci.* **4**, 426 (2017).
36. Hemming, S. R. New K/Ar age values and context from published clay mineralogy and Sr and Nd isotopes as tracers of terrigenous Atlantic Ocean sediments. *Mar. Geol.* **411**, 36–50 (2019).
37. Pöppelmeier, F. et al. Neodymium isotopes as a paleo-water mass tracer: a model-data reassessment. *Quat. Sci. Rev.* **279**, 107404 (2022).
38. Lacan, F. & Jeandel, C. Neodymium isotopes as a new tool for quantifying exchange fluxes at the continent–ocean interface. *Earth Planet. Sci. Lett.* **232**, 245–257 (2005).
39. Koenigk, T. & Brodeau, L. Arctic climate and its interaction with lower latitudes under different levels of anthropogenic warming in a global coupled climate model. *Clim. Dyn.* **49**, 471–492 (2017).
40. Neff, A., Keane, A., Dijkstra, H. A. & Krauskopf, B. Bifurcation analysis of a North Atlantic Ocean box model with two deep-water formation sites. *Phys. Nonlinear Phenom.* **456**, 133907 (2023).
41. Elderfield, H. et al. Evolution of ocean temperature and ice volume through the mid-pleistocene climate transition. *Science* **337**, 704–709 (2012).
42. Frank, M., Whiteley, N., Kasten, S., Hein, J. R. & O'Nions, K. North Atlantic Deep Water export to the Southern Ocean over the past 14 Myr: evidence from Nd and Pb isotopes in ferromanganese crusts. *Paleoceanography* **17**, 12-1 (2002).
43. Jeandel, C. Overview of the mechanisms that could explain the 'Boundary Exchange' at the land–ocean contact. *Philos. Trans. R. Soc. Math. Phys. Eng. Sci.* **374**, 20150287 (2016).
44. McClymont, E. L. et al. Lessons from a high-CO_2 world: an ocean view from ~3 million years ago. *Clim. Past* **16**, 1599–1615 (2020).
45. Sosdian, S. M. & Rosenthal, Y. Deep-sea temperature and ice volume changes across the Pliocene-Pleistocene climate transitions. *Science* **325**, 306–310 (2009).
46. Burls, N. J. et al. Active Pacific meridional overturning circulation (PMOC) during the warm Pliocene. *Sci. Adv.* **3**, e1700156 (2017).
47. Shankle, M. G. et al. Pliocene decoupling of equatorial Pacific temperature and pH gradients. *Nature* **598**, 457–461 (2021).
48. Ford, H. L. et al. Sustained mid-Pliocene warmth led to deep water formation in the North Pacific. *Nat. Geosci.* **15**, 658–663 (2022).
49. Saenko, O. A., Schmittner, A. & Weaver, A. J. The Atlantic–Pacific seesaw. *J. Clim.* **17**, 2033–2038 (2004).
50. Menviel, L. C., England, M. H., Meissner, K. J., Mouchet, A. & Yu, J. Atlantic-Pacific seesaw and its role in outgassing CO_2 during Heinrich events: Heinrich CO_2. *Paleoceanography* **29**, 58–70 (2014).
51. Baker, J. A. et al. Continued Atlantic overturning circulation even under climate extremes. *Nature* **638**, 987–994 (2025).
52. Marshall, J. & Schott, F. Open-ocean convection: observations, theory, and models. *Rev. Geophys.* **37**, 1–64 (1999).
53. Woodard, S. C. et al. Antarctic role in Northern Hemisphere glaciation. *Science* **346**, 847–851 (2014).
54. Zhao, N. et al. Glacial–interglacial Nd isotope variability of North Atlantic Deep Water modulated by North American ice sheet. *Nat. Commun.* **10**, 5773 (2019).
55. Du, J., Haley, B. A. & Mix, A. C. Evolution of the Global Overturning Circulation since the Last Glacial Maximum based on marine authigenic neodymium isotopes. *Quat. Sci. Rev.* **241**, 106396 (2020).
56. Williams, T. J. et al. The role of ocean circulation and regolith removal in triggering the Mid-Pleistocene transition: insights from authigenic Nd isotopes. *Quat. Sci. Rev.* **345**, 109055 (2024).
57. Newsom, E. R., Thompson, A. F., Adkins, J. F. & Galbraith, E. D. A hemispheric asymmetry in poleward ocean heat transport across climates: Implications for overturning and polar warming. *Earth Planet. Sci. Lett.* **568**, 117033 (2021).
58. Clark, P. U., Shakun, J. D., Rosenthal, Y., Köhler, P. & Bartlein, P. J. Global and regional temperature change over the past 4.5 million years. *Science* **383**, 884–890 (2024).
59. Frajka-Williams, E., Foukal, N. & Danabasoglu, G. Should AMOC observations continue: how and why? *Philos. Trans. R. Soc. Math. Phys. Eng. Sci.* **381**, 20220195 (2023).
60. In *Proceedings of the Ocean Drilling Program, 154 Initial Reports*. 154 (Ocean Drilling Program, 1995).
61. Howe, J. N. W. et al. North Atlantic Deep Water Production during the Last Glacial Maximum. *Nat. Commun.* **7**, 11765 (2016).
62. Howe, J. N. W. & Piotrowski, A. M. Atlantic deep water provenance decoupled from atmospheric CO_2 concentration during the lukewarm interglacials. *Nat. Commun.* **8**, 2003 (2017).
63. GEOTRACES Intermediate Data Product Group. The GEOTRACES Intermediate Data Product 2021 version 2 (IDP2021v2). *NERC EDS British Oceanographic Data Centre NOC* https://doi.org/10.5285/FF46F034-F47C-05F9-E053-6C86ABC0DC7E (2023).
64. *Proceedings of the Ocean Drilling Program, 181* Initial Reports. 181 (Ocean Drilling Program, 2000).

65. Hodell, D. A. Late Pleistocene Paleoceanography of the South Atlantic Sector of the Southern Ocean: Ocean Drilling Program Hole 704A. *Paleoceanography* **8**, 47–67 (1993).
66. Hu, R. & Piotrowski, A. M. Neodymium isotope evidence for glacial-interglacial variability of deepwater transit time in the Pacific Ocean. *Nat. Commun.* **9**, 4709 (2018).
67. Curry, W. B., Shackleton, N. J. & Richter, C. Site 925. In *Proceedings of the Ocean Drilling Program, 154 Initial Reports* 154 (Ocean Drilling Program, 1995).
68. Kumar, N. & Embley, R. W. Evolution and origin of Ceará Rise: an aseismic rise in the western equatorial Atlantic. *Geol. Soc. Am. Bull.* **88**, 683 (1977).
69. van Soelen, E. E. et al. A 30 Ma history of the Amazon River inferred from terrigenous sediments and organic matter on the Ceará Rise. *Earth Planet. Sci. Lett.* **474**, 40–48 (2017).
70. Stewart, J. A., Gutjahr, M., James, R. H., Anand, P. & Wilson, P. A. Influence of the Amazon River on the Nd isotope composition of deep water in the western equatorial Atlantic during the Oligocene–Miocene transition. *Earth Planet. Sci. Lett.* **454**, 132–141 (2016).
71. Carter, R. M. et al. Site 1123: North Chatham Drift - A 20-Ma Record of the Pacific Deep Western Boundary Current. In *Proceedings of the Ocean Drilling Program, 181 Initial Reports* (eds Carter, R. M. et al.) 181 (Ocean Drilling Program, 2000).
72. Elderfield, H. et al. A record of bottom water temperature and seawater δ18O for the Southern Ocean over the past 440kyr based on Mg/Ca of benthic foraminiferal Uvigerina spp. *Quat. Sci. Rev.* **29**, 160–169 (2010).
73. Frost, C. & Coombs, D. Nd isotope character of New Zealand sediments; implications for terrane concepts and crustal evolution. *Am. J. Sci.* **289**, 744–770 (1989).
74. Pickett, D. A. & Wasserburg, G. Neodymium and strontium isotopic characteristics of New Zealand granitoids and related rocks. *Contrib. Mineral. Petrol.* **103**, 131–142 (1989).
75. Hodell, D. A. & Warnke, D. A. Climatic evolution of the Southern Ocean during the Pliocene epoch from 4.8 to 2.6 million years ago. *Quat. Sci. Rev.* **10**, 205–214 (1991).
76. Tanaka, T. et al. JNdi-1: a neodymium isotopic reference in consistency with LaJolla neodymium. *Chem. Geol.* **168**, 279–281 (2000).
77. Weis, D. et al. High-precision isotopic characterization of USGS reference materials by TIMS and MC-ICP-MS. *Geochem. Geophys. Geosystems* **7** (2006).
78. Wilkens, R. H. et al. Revisiting the Ceara Rise, equatorial Atlantic Ocean: isotope stratigraphy of ODP Leg 154 from 0 to 5 Ma. *Clim. Past* **13**, 779–793 (2017).
79. Lisiecki, L. E. & Raymo, M. E. A Pliocene-Pleistocene stack of 57 globally distributed benthic δ^{18}O records: PLIOCENE-PLEISTOCENE BENTHIC STACK. *Paleoceanography* **20**, 1–17 (2005).
80. Patterson, M. O. et al. A Southwest Pacific Perspective on long-term global trends in Pliocene-Pleistocene stable isotope records. *Paleoceanogr. Paleoclimatol.* **33**, 825–839 (2018).
81. Burke, M. D. A Gaussian Bootstrap Approach to Estimation and Tests. In *Asymptotic Methods in Probability and Statistics* 697–706 https://doi.org/10.1016/B978-044450083-0/50045-9 (Elsevier, 1998).
82. de Graaf, F. FmDG/Transects: publication release. *Zenodo* https://doi.org/10.5281/ZENODO.17513046 (2025).
83. GEBCO Bathymetric Compilation Group 2024. The GEBCO_2024 Grid—a continuous terrain model of the global oceans and land. *NERC EDS British Oceanographic Data Centre NOC* https://doi.org/10.5285/1C44CE99-0A0D-5F4F-E063-7086ABC0EA0F (2024).
84. Schlitzer, R. Ocean Data View (2025).

Acknowledgements

We thank E. Humphreys-Williams and M. Stanley for their laboratory assistance, and the International Ocean Discovery Program and R. Tiedemann and T. Bickert for providing the samples.

Author contributions

F.d.G., D.J.W. and H.L.F. designed the study. F.d.G., Z.H. and S.W. carried out the geochemical analysis. The data were analysed by F.d.G. with assistance from D.T., D.J.W., Y.R., S.W., and H.L.F. F.d.G., D.T., D.J.W., Z.H., Y.R., S.W. and H.L.F. contributed to the final manuscript.

Funding

F.d.G. was supported by the London Natural Environmental Research Council (NERC) Doctoral Training Partnership (NE/S007229/1) and by a grant from the Geological Society of London. D.T. received funding from the Leverhulme Trust. D.J.W. was supported by a NERC independent research fellowship (NE/T011440/1). Y.R. and S.W. were supported by the US National Science Foundation (OCE-1334691). H.L.F. was supported by NERC (NE/N015045/1).

Competing interests

The authors declare no competing interests.

Additional information

Supplementary information The online version contains supplementary material available at https://doi.org/10.1038/s41467-026-79566-7.

Correspondence and requests for materials should be addressed to Friso de Graaf.

Peer review information *Nature Communications* thanks Helen Coxall and the other, anonymous, reviewer(s) for their contribution to the peer review of this work. A peer review file is available.

Reprints and permissions information is available at http://www.nature.com/reprints

Publisher's note Springer Nature remains neutral with regard to jurisdictional claims in published maps and institutional affiliations.

Open Access This article is licensed under a Creative Commons Attribution-NonCommercial-NoDerivatives 4.0 International License, which permits any non-commercial use, sharing, distribution and reproduction in any medium or format, as long as you give appropriate credit to the original author(s) and the source, provide a link to the Creative Commons licence, and indicate if you modified the licensed material. You do not have permission under this licence to share adapted material derived from this article or parts of it. The images or other third party material in this article are included in the article's Creative Commons licence, unless indicated otherwise in a credit line to the material. If material is not included in the article's Creative Commons licence and your intended use is not permitted by statutory regulation or exceeds the permitted use, you will need to obtain permission directly from the copyright holder. To view a copy of this licence, visit http://creativecommons.org/licenses/by-nc-nd/4.0/.

© The Author(s) 2026

This Article in Press is shared early to give you faster access to new research. It is citable and carries a permanent DOI. The final edited version will replace it automatically.